WILEY

RESEARCH ARTICLE OPEN ACCESS

Investigating the Human Brain's Integration of Internal and External Reference Frames: The Role of the Alpha and Beta Bands in a Modified Temporal Order Judgment Task

Xianhao Wei[1,2] 🔟 | Jian Zhang[3] 🔟 | Jinyan Zhang[3] 🔟 | Zimo Li[4] | Qi Li[1,5] 🔟 | Jinglong Wu[2,3,4] | Jingjing Yang[6] 🔟 | Zhilin Zhang[2] 🔟

[1]School of Computer Science and Technology, Changchun University of Science and Technology, Changchun, China | [2]Research Center for Medical Artificial Intelligence, Shenzhen Institute of Advanced Technology, Chinese Academy of Sciences, Shenzhen, China | [3]School of Medical Technology, Beijing Institute of Technology, Beijing, China | [4]Graduate School of Interdisciplinary Science and Engineering in Health Systems, Okayama University, Okayama, Japan | [5]Zhongshan Institute of Changchun University of Science and Technology, Zhongshan, China | [6]School of Artificial Intelligence, Changchun University of Science and Technology, Changchun, China

Correspondence: Qi Li (liqi@cust.edu.cn) | Zhilin Zhang (zhangzhilin@siat.ac.cn)

ABSTRACT

The integration of the internal and external reference frames of the human brain is crucial for achieving accurate tactile spatial localization. However, the mechanisms underlying this integration have yet to be fully elucidated. This study adopted a modified temporal order judgment paradigm with an advanced weighted phase lag index method to investigate brain network interactions when the internal and external reference frames were integrated. We found that when the brain integrated internal and external reference frames, alpha oscillations decreased, beta oscillations increased, and inter-hemispheric connectivity increased. Specifically, compared with the match condition: first, the alpha band oscillation predominantly contributed to processing the internal reference frame mismatch; second, the alpha and late beta band oscillation predominantly contributed to processing the external reference frame mismatch; third, the early alpha and late beta band oscillation predominantly contributed to processing the internal and external reference frame mismatch. These findings suggest that the neural oscillation of the alpha and beta bands plays an essential role in tactile spatial localization.

1 | Introduction

Humans, as well as several nonhuman species, are able to localize a touch in space. This ability often requires the integration of internal and external reference frames. The internal reference frame primarily comprises somatotopic representations where the tactile stimulus occurs on the skin (Haggard et al. 2003; Penfield and Boldrey 1937; Roux et al. 2018; Serino and Haggard 2010). In contrast, the external reference frame is composed primarily of spatiotopic representations where the position of the stimulated limbs is in the external space (Azañón et al. 2015; Heed et al. 2015; Yamamoto and Kitazawa 2001). To perceive the location of the stimulus and take action, the brain must not only identify which part of the

---

body is in contact with tactile stimuli but also locate these stimuli in the surrounding environment (Azañón et al. 2015; Heed and Azañon 2014; Heed et al. 2015; Overvliet et al. 2011).

Temporal order judgment (TOJ) is typically used to explore how the brain integrates internal and external reference frames to localize tactile stimuli in space (Heed and Azañón 2014; Sambo et al. 2013). In the TOJ task, participants receive two rapid and sequential stimuli on both the left and right hands and are asked to immediately judge the order of the stimuli. With uncrossed hands (default posture), participants can discriminate stimulus order accurately even at very short time intervals (~30–70 ms). However, when the hands are crossed over the body midline, performance becomes significantly impaired, and a larger time interval is required between stimuli for correct performance (~120–300 ms) (Sambo et al. 2013; Schicke and Röder 2006; Shore et al. 2002; Yamamoto and Kitazawa 2001). These findings suggest that the somatotopic representation mismatches the spatiotemporal representation (e.g., a stimulus applied on the left hand of the internal reference frame coming from the right part of the external reference frame, and vice versa), thereby impairing the ability to correctly judge the localization of tactile stimuli in space. Moreover, the crossing effect is reliable and stable, as it persists even when the two tactile stimuli differ in frequency or duration (Heed and Azañón 2014; Sambo et al. 2013; Shore et al. 2002; Yamamoto and Kitazawa 2001). However, previous studies have focused only on the mismatch between internal and external reference frames, while the mismatches within internal and external reference frames to localize tactile stimuli in space have yet to be fully elucidated.

In this study, we employed a modified TOJ paradigm involving mismatches within internal and external reference frames to elucidate the neural mechanisms underlying tactile spatial processing. The participants received two rapid and sequential stimuli on both the hand and the foot and were asked to judge the order of the stimuli from the hand to the foot or vice versa. In the mismatch of the internal reference frame condition, two tactile stimuli were delivered to different body sides, such as the left hand with the right foot or the right hand with the left foot combinations. The participants needed to integrate skin-based tactile information across different body sides for TOJ. Compared with the limbs on the opposite sides of the body, the limbs on the same side are more likely to be part of a unified internal system. As demonstrated by behavioral data, a touch is more likely to be misattributed to the same side of the body than to the opposite side of the body (Badde et al. 2019). In terms of the mismatch of the external reference frame condition, two stimuli are delivered to different sides of the external space, such as the left hand and the right foot combination if the hands and foot are placed on their default (uncross) side of the external place or the right hand crossed over the body midline and the right foot combination if the hands and foot are placed on the crossed side of the external place. This setup requires participants to integrate tactile information across the body midline to make a temporal judgment. Compared with stimuli presented on the same side of the external space, stimuli on opposite sides are less likely to be perceived as part of a unified external spatial system, as processing tactile information across different sides of the external space can lead to increased errors and thresholds (Ritterband-Rosenbaum et al. 2014; Tamè et al. 2019). This modified TOJ paradigm, which involves tactile stimuli presented across different sides of the body

and external space, allows us to assess mismatches separately within internal and external reference frames. By identifying the distinct contributions and challenges associated with each reference frame, this approach can enhance our understanding of tactile spatial processing.

Electroencephalography (EEG) has long been considered to have excellent temporal resolution for studying brain activity (Hassan and Wendling 2018; O'Neill et al. 2018). Rhythmic brain activity in the alpha (8–15 Hz) and beta (17–25 Hz) frequency bands is influenced by sensorimotor tasks (Cheyne et al. 2003). Researchers have reported that oscillations in the alpha and beta bands are related to tactile localization in the integration of internal and external reference frames, with these reference frames being self-centered (Buchholz et al. 2011; Heed et al. 2015). Recent studies have suggested that the integration of internal and external reference frames involves dynamic functional connectivity of alpha and beta regions in brain networks (Moharramipour et al. 2023). To capture the complexity of brain networks, the weighted phase lag index (WPLI) is utilized for functional connectivity analysis (Imperatori et al. 2019; Lau et al. 2012; Xie et al. 2022). Specifically, the WPLI is employed to construct phase synchronization networks from EEG signals, which are then converted into functional connectivity networks for analyzing brain network interactions. The WPLI cannot overestimate the phase lag values because of the volume conduction effects of uncorrelated noise sources. Therefore, the WPLI is reported to be less sensitive to noise than the traditional PLI, and even under conditions of a high signal-to-noise ratio, it has a more reliable relationship with true phase consistency (Stam et al. 2007). This characteristic makes the WPLI a suitable tool for exploring phase synchronization relationships across the brain network in different frequency bands, leading to more reliable insights into the neural mechanisms underlying the integration of internal and external reference frames.

In this study, we adopted a modified TOJ paradigm with an advanced WPLI method to investigate the neural oscillation of the brain network when the internal and external reference frames are mismatched and what in these networks contributes to localizing tactile stimuli in space. We delivered rapid, sequential electrical stimulation to the hand and foot and asked participants to judge the order of the stimuli, with the hand and foot stimulation positions following these conditions: (1) different versus same body sides to examine brain network interactions associated with mismatches within the internal reference frames, (2) different versus same sides of the external space to explore network interactions related to mismatches within external reference frames, and (3) hand crossing the body midline versus default position to investigate brain network interactions during the integration of mismatches between internal and external reference frames.

2 | Materials and Methods

2.1 | Participants

Twenty-nine right-handed adults (12 males and 17 females, ranging in age from 21 to 33 years, mean ± SD: 25.2 ± 3.0 years) participated in our study. Handedness was determined on the

basis of the Edinburgh Handedness Inventory (Oldfield 1971). The sample size was determined a priori using G*Power v.3.1 to estimate the number of participants needed to detect significant effects with 80% statistical power (Faul et al. 2007). With the assumption of a matched samples *t*-test, an effect size of dz = 0.6, a type I error probability of $\alpha = 0.05$, and an analytical power of $(1 - \beta) = 0.80$, we needed a minimum sample of 24 participants. Our sample size was greater than the estimated sample size needed. All participants were physically healthy without any motor or sensory impairments. All participants signed an informed consent form in advance, and the entire procedure of the experiment was clearly explained to each participant before EEG data collection. The experiment was approved by the ethics committee of the Shenzhen Institute of Advanced Technology, Chinese Academy of Sciences.

2.2 | Experimental Paradigm

Before the experiment, a Digitimer DS7A Constant Current Stimulator (Digitimer Ltd., Welwyn Garden City, UK) was used to determine the stimulation intensity at four electrical stimulation sites for each participant: the second joint of the left middle finger, the second joint of the right middle finger, the area above the left ankle joint, and the area above the right ankle joint. The stimulation intensity at the four sites was set at 1.5-fold the minimal intensity perceived at each body site (Alouit et al. 2024; Williamson et al. 2022). The minimal intensity perceived was defined as the lowest intensity detected by the participant in all 10 out of 10 consecutive stimuli, with the intensity increasing from 1 in 0.1-mA intervals (Rocchi et al. 2016). The stimulation current used in the experiment consisted of a single square wave pulse with a duration of 0.2 ms (Williamson et al. 2022).

The participants subsequently performed a tactile TOJ task involving internal and external reference frames while their EEG data were recorded. Figure 1A illustrates the experimental paradigm. At the beginning of the experiment, the participants received a randomly ordered sequence of the eight electrical stimulation postures shown in Figure 1B, which they adopted sequentially according to the assigned order. In each posture, the participants fixated on a white cross on the screen. After an intertrial interval of 1200–3000 ms, the participants received two sequential electrical stimuli with 15 random interstimulus interval (ISI) situations (ISI ranging from −350 ms to +350 ms in 50-ms steps). An ISI of 0 ms indicated that the two stimuli were presented simultaneously. The "+" indicates the hand before the foot, and the "−" indicates the opposite. The participants completed 120 trials in each posture, consisting of eight sets, each with 15 different randomized ISI conditions. This approach ensured that each ISI was randomly presented eight times within each posture. When the second stimulus of each trial appeared, participants had a 2000-ms window to make a forced-choice response and to judge whether the sequence of events was "hand first, foot second" or "foot first, hand second." The "1" and "3" keys on the keyboard were designated response keys, and the key mapping was balanced across participants. After making a judgment, the participants immediately proceeded to the next trial. If participants did not respond within the 2000-ms window,

the next trial began automatically. Each participant ultimately completed the TOJ task across eight postures (blocks), totaling 960 trials. A 5-min break was provided between each block.

The overall experiment and the three experimental conditions are shown in Figure 1. The participants were required to complete the modified TOJ experiment shown in Figure 1A, following the eight different postures in a pseudorandom order displayed in Figure 1B. We subsequently analyzed the task-related EEG data on the basis of the three conditions in Figure 1C.

2.3 | EEG Data Collection and Analysis

2.3.1 | Data Collection and Preprocessing

We processed the 32-channel EEG data related to the task (using the Grael 4K EEG Amplifier, standard Ag/AgCl electrodes placed on the scalp according to the international 10-20 frame, with impedance reduced to 10 kΩ) by applying a notch filter at 50 Hz to remove power line interference, followed by bandpass from 0.1 to 40 Hz. We downsampled the 1024-Hz EEG data to 200 Hz. Independent component analysis was employed to eliminate electrooculograms, electrocardiograms, electromyograms, and other artifacts. We then rereferenced the data via the M1 and M2 electrodes. Finally, we segmented the data according to the eight different electrical stimulation postures (excluding bad segments) and performed baseline correction. All neurophysiological data analyses were conducted using the MNE toolbox (Gramfort et al. 2013).

2.3.2 | Functional Connectivity Analysis

In the present study, a functional connectivity method called the WPLI was implemented (Vinck et al. 2011). The WPLI measures the nondirectional coupling between two electrodes across time and frequency as follows:

$$S_{ij}(f,t) = x_i(f,t)x_j^*(f,t) \tag{1}$$

$$\mathrm{WPLI}_{ij}(f,t) = \left| \frac{\sum_{m=1}^{n} \left| \mathrm{Im}\left(S_{ij}(f,t)_m\right) \right| \mathrm{sgn}\left(\mathrm{Im}\left(S_{ij}(f,t)_m\right)\right)}{\sum_{m=1}^{n} \left| \mathrm{Im}\left(S_{ij}(f,t)_m\right) \right|} \right| \tag{2}$$

where f and t represent frequency and time, respectively; x_i and x_j are the time–frequency transformed data of the EEG signals from the i-th and j-th electrodes during one trial; S_{ij} is their cross-spectrum; Im represents the imaginary part of a complex value; sgn() is the sign function, which returns 1 if $\mathrm{Im}\left(S_{ij}(f,t)_m\right) > 0$, 0 if $\mathrm{Im}\left(S_{ij}(f,t)_m\right) = 0$, and −1 if $\mathrm{Im}\left(S_{ij}(f,t)_m\right) < 0$; and n is the number of trials. If there is a meaningful consistent phase lag between two EEG signals across trials, they are considered coupled. The WPLI value ranges from 0 to 1, and stronger coupling is indicated by higher WPLI values. We calculated the WPLI for each of the 496 connectivity pairs across the 32 electrodes, with frequencies ranging from 5 to 30 Hz (every 1 Hz) and times ranging from −400 to 1200 ms (every 5 ms) (e.g., Figure 2B). A time of 0s corresponds to when the participant first received
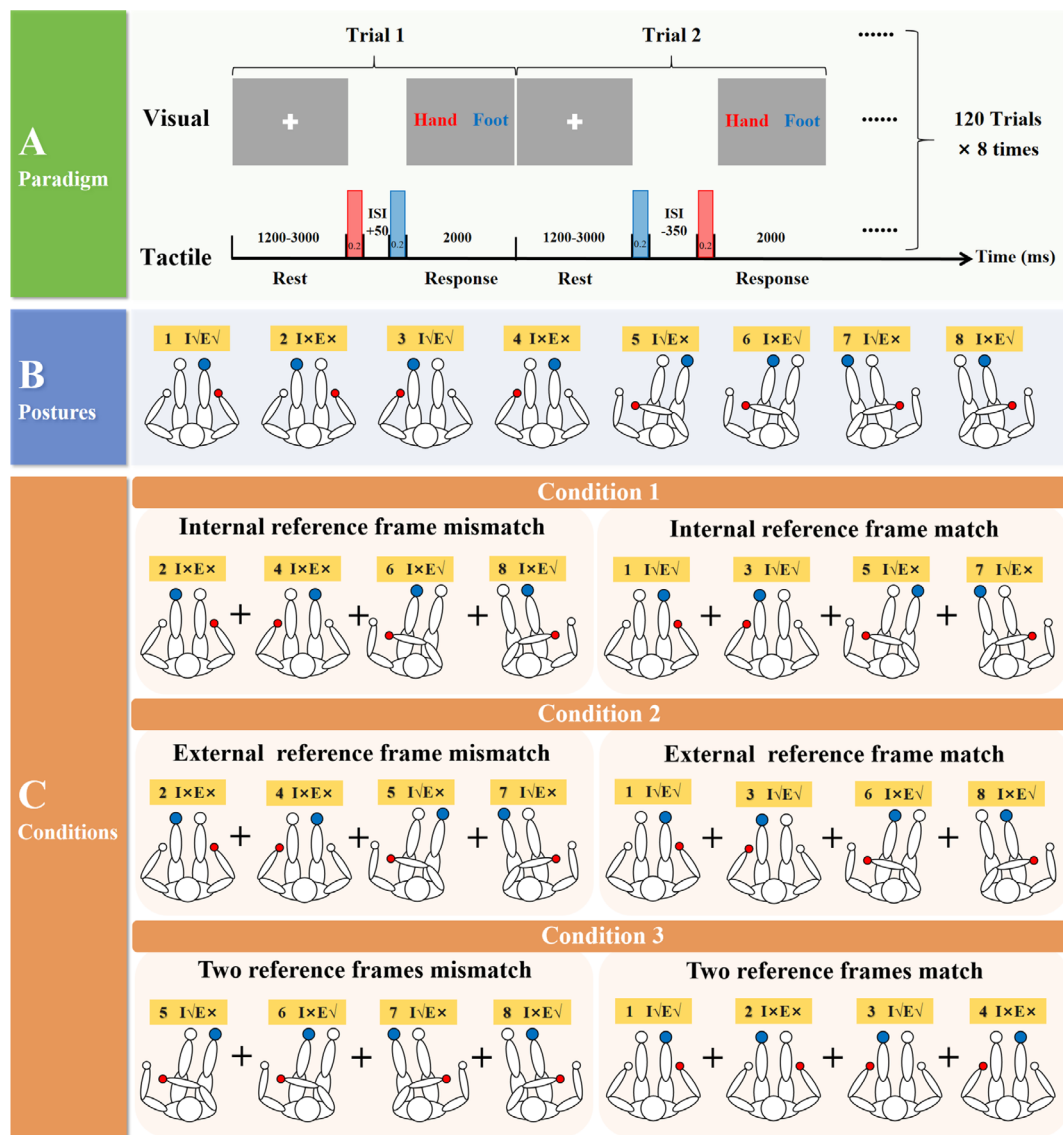
FIGURE 1 | Schematic of the experimental paradigm, eight postures, and three conditions. (A) The experimental paradigm, where participants judged the order of two rapidly delivered sequential stimuli to the hand and foot. The red rectangle represents hand stimulation, and the blue rectangle represents foot stimulation. (B) The eight different electrical stimulation postures. Numbers 1–8 represent the eight different electrical stimulation postures. The uppercase letter "I" represents the internal reference frame, and "E" represents the external reference frame. The check mark ($\sqrt{}$) indicates a match, and the cross ($\times$) indicates a mismatch. (C) The three conditions.

electrical stimulation. For time–frequency calculations of the EEG data, we applied the wavelet time–frequency analysis method from the MNE toolbox (Cohen 2019). We adopted a common approach to determine the number of cycles in wavelet time–frequency analysis, which starts with fewer cycles at lower frequencies and gradually increases the number of cycles as the frequency increases (Morales and Bowers 2022). This strategy increases temporal precision at lower frequencies and strengthens frequency precision at higher frequencies, balancing both temporal and frequency precision.

We standardized the WPLI values at the individual participant level at each frequency row via z-score normalization (mean $= 0$, SD $= 1$). The normalization was applied independently on each frequency, as the distribution of the WPLI value usually varied across frequencies. The normalization can help better detect the

couplings' evolution during the task across the participants. Thus, it would improve the identification of task-related couplings. Figure 2C shows an example of the normalized WPLI (NWPLI) at each time–frequency bin averaged across the participants.

2.3.3 | Statistical Analysis

To derive the brain network (couplings) that emerged after the delivery of the first tactile stimulus (0 ms), we applied the following statistic to the time–frequency NWPLI values of the participants. First, the median of the NWPLI value during the prestimulus period (−400 to 0 ms) was calculated for each participant and at each frequency:

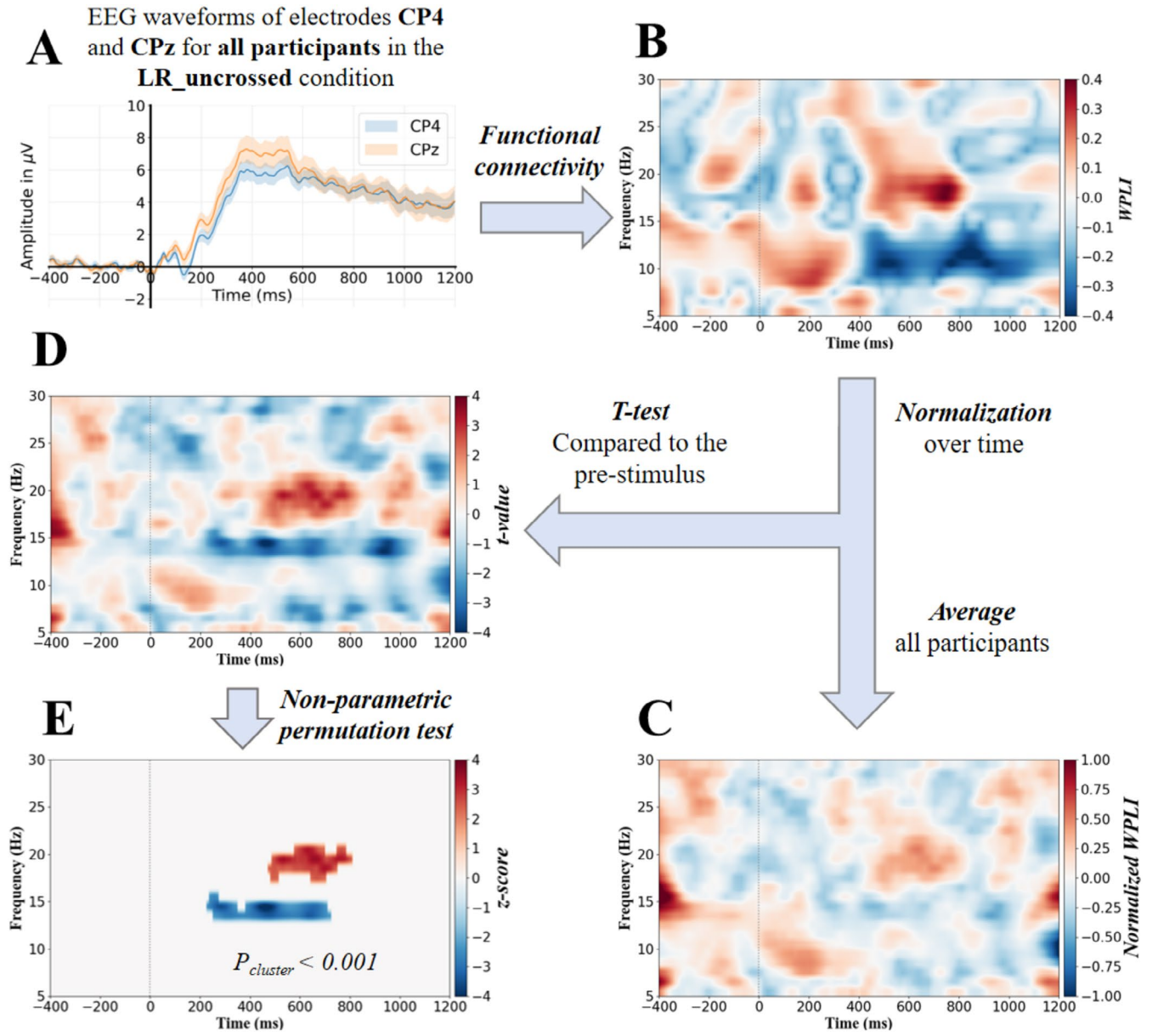$$X_{f,t} = \text{NWPLI}(f, t) \text{ of each subject}$$

FIGURE 2 | Summary of the EEG functional connectivity analysis. (A) EEG waveforms of electrodes CP4 and CPz under the LR_uncrossed (Figure 1B fourth) situation for all participants. The solid line and shaded area represent the mean and standard error of all trials, respectively. The dashed line indicates the time of the first tactile stimulus. (B) The time–frequency WPLI was calculated between the electrodes shown in (A). (C) The normalized WPLI (NWPLI) was obtained through normalization of the WPLI of B at each frequency, followed by averaging the data across participants. (D) The t-statistic was calculated at the group participant level at each frequency between each NWPLI bin and the median of the prestimulus NWPLI (Equation 3). (E) The significant time–frequency cluster of (D) was detected by the nonparametric permutation statistical test.

$$X_f^{\mathrm{B}} = \mathrm{median}\left(X_{f,t<0}\right) \quad (3)$$

Then, Welch's t-statistic was calculated from the mean and variance of $X_{f,t}$ and X_f^{B} as follows (e.g., Figure 2D):

$$t_{f,t} = \frac{E\left(X_{f,t}\right) - E\left(X_f^{\mathrm{B}}\right)}{\sqrt{\frac{\mathrm{var}\left(X_{f,t}\right)}{N_{\mathrm{s}}} + \frac{\mathrm{var}\left(X_f^{\mathrm{B}}\right)}{N_{\mathrm{s}}}}} \quad (4)$$

where $E()$ and var() indicate the mean and variance across participants, and N_{s} is the number of participants. Notably, Welch's t-statistic is more reliable than Student's t-statistic among

samples with unequal variances, which were the case in our study (Ruxton 2006).

To identify the significant time–frequency clusters on the t-statistic maps (e.g., Figure 2D), we applied a nonparametric permutation test (Maris and Oostenveld 2007). In each permutation, the t-statistic was calculated after randomly permuting the NWPLI values and the median of the NWPLI during the prestimulus period (i.e., $X \leftrightarrow X^{\mathrm{B}}$) across participants. The null distribution of the t-statistic was then empirically derived using all the t-statistics that were calculated by the large number of permutation sets (99,200) (Moharramipour et al. 2023). For each permutation set, the time–frequency clusters whose t-statistic

was smaller than the 2.5th or greater than the 97.5th of the null distribution were identified. Subsequently, the clusters with the overall maximum positive and minimum negative t statistics were identified. This process was repeated for all the permutation sets, and the histogram of the maximum/minimum cluster t-values was acquired. This histogram corresponds to the null hypothesis in which there should be no time–frequency cluster of connectivity significantly altered by the stimuli. Finally, the threshold for a significant cluster t-value was determined by using this histogram and a specified alpha threshold (P_c) (i.e., the probability of falsely detecting a cluster as significant). Moreover, we accounted for another secondary multiple comparisons problem at the network level by applying the Bonferroni correction. In this correction, since there were 496 connectivity pairs, the alpha threshold needed to be divided by 496. The alpha thresholds of 0.05/496 (Bonferroni correction), 0.001, and 0.05 were employed in the present study.

We present the results of the statistical test in the form of a z-score (e.g., Figure 2E) as follows:

$$z - \text{score} = \text{CDF}_{\text{normal}}^{-1}\big(\text{CDF}_t(t - \text{value})\big) \qquad (5)$$

where CDF_t is the cumulative distribution function of the empirically derived null distribution of the t-statistic, and where CDF_{normal}^{-1} is the inverse of the normal cumulative distribution function, which transforms the P-value of the t-test into a z-score. Transforming the test outcome into z-scores enables a fair comparison of different experimental conditions because their empirically derived t-statistic null distributions are not necessarily the same (i.e., they could be slightly wider or tighter).

To show the overall behavior (i.e., density) of the brain network over time and frequency (e.g., Figure 3A), we summed the task-related z-scores (e.g., Figure 2E) of all 496 connectivity pairs ($P_c < 0.05$). Furthermore, we statistically compared the network density difference between the experimental conditions across time and frequency via the Wilcoxon signed-rank test (Hollander et al. 2013) (e.g., Figure 3E). At each time–frequency point, the Wilcoxon signed-rank test ($p < 0.05$) was applied to the z-scores of 496 connectivity pairs of two different conditions. Then, the significant time–frequency clusters were identified via the nonparametric permutation test (Maris and Oostenveld 2007), similar to what was explained previously ($P_c < 0.05$). Next, we plotted the brain networks associated with the time window of 200–800ms and the frequency range of 8–15Hz for the alpha band, and the brain networks associated with the time window of 400–900ms and the frequency range of 17–25Hz for the beta band, as shown in Figure 3B and Figure 3D, respectively. Magenta and cyan colors indicate the connections that pass the test with a P_c smaller than 0.05/496 (Bonferroni correction) and 0.001, respectively.

Moreover, we selected the connections passing the test ($P_c < 0.05/496$ [Bonferroni correction]) and applied the Wilcoxon signed-rank test ($p < 0.05$) separately to each node of the network to identify those nodes with significant density differences between the two experimental conditions. For each electrode, the test was applied to the z-scores of its 31 connectivity pairs with the other electrodes across conditions, and the significant electrodes are marked with red dashed circles.

We analyzed the EEG data of all the participants following the aforementioned procedures, and the processed data were summarized under the following three conditions: internally reference frame mismatch versus internally reference frame match; externally reference frame mismatch versus externally reference frame match; two reference frames mismatch versus two reference frames match (Figures 1–3C).

Under each condition, we identified significant differences in the alpha and beta bands (see Figures 3E, 4E, and 5E). To verify whether the alpha and beta bands are related to the results, we performed Pearson correlation analysis under each condition to explore the relationship between the significant differences in these bands and accuracy differences.

$$\Delta C_{\text{band}} = C_{\text{band,match}} - C_{\text{band,mismatch}} \qquad (6)$$

$$\Delta \text{Acc} = \text{Acc}_{\text{match}} - \text{Acc}_{\text{mismatch}} \qquad (7)$$

where $C_{\text{band,match}}$ represents the total coupling of the alpha or beta band under the match condition, and $C_{\text{band,mismatch}}$ represents the total coupling of the alpha or beta band under the mismatch condition. ΔC_{band} represents the difference in total coupling between the two conditions. $\text{Acc}_{\text{match}}$ represents the accuracy under the match condition, and $\text{Acc}_{\text{mismatch}}$ represents the accuracy under the mismatch condition. ΔAcc represents the difference in accuracy between the two conditions.

For Condition 1:

$$r\big(\Delta C_\alpha, \Delta \text{Acc}\big) \qquad (8)$$

where r represents the correlation between the two variables and ΔC_α under Condition 1 represents the difference in total coupling of the alpha band between the internal reference frame mismatch and match conditions, where α refers to the coupling selected from the time window of 350–800ms and frequency band of 8–10Hz, as well as the time window of 520–660ms and frequency band of 13–15Hz. ΔAcc represents the difference in accuracy between the internal reference frame mismatch and match conditions.

For Condition 2:

$$r\big(\Delta C_\alpha + \Delta C_\beta, \Delta \text{Acc}\big) \qquad (9)$$

where r represents the correlation between the two variables and ΔC_α under Condition 2 represents the difference in total coupling of the alpha band between the external reference frame mismatch and match conditions, where α refers to the coupling selected from the time window of 200–700ms and frequency band of 13–15Hz. ΔC_β under Condition 2 represents the difference in total coupling of the beta band between the external reference frame mismatch and match conditions, where β refers to the coupling selected from the time window of 750–900ms and frequency band of 17–25Hz. ΔAcc represents the difference in accuracy between the external reference frame mismatch and match conditions.

For Condition 3:

$$r\big(-\Delta C_\alpha + \Delta C_\beta, \Delta \text{Acc}\big) \qquad (10)$$
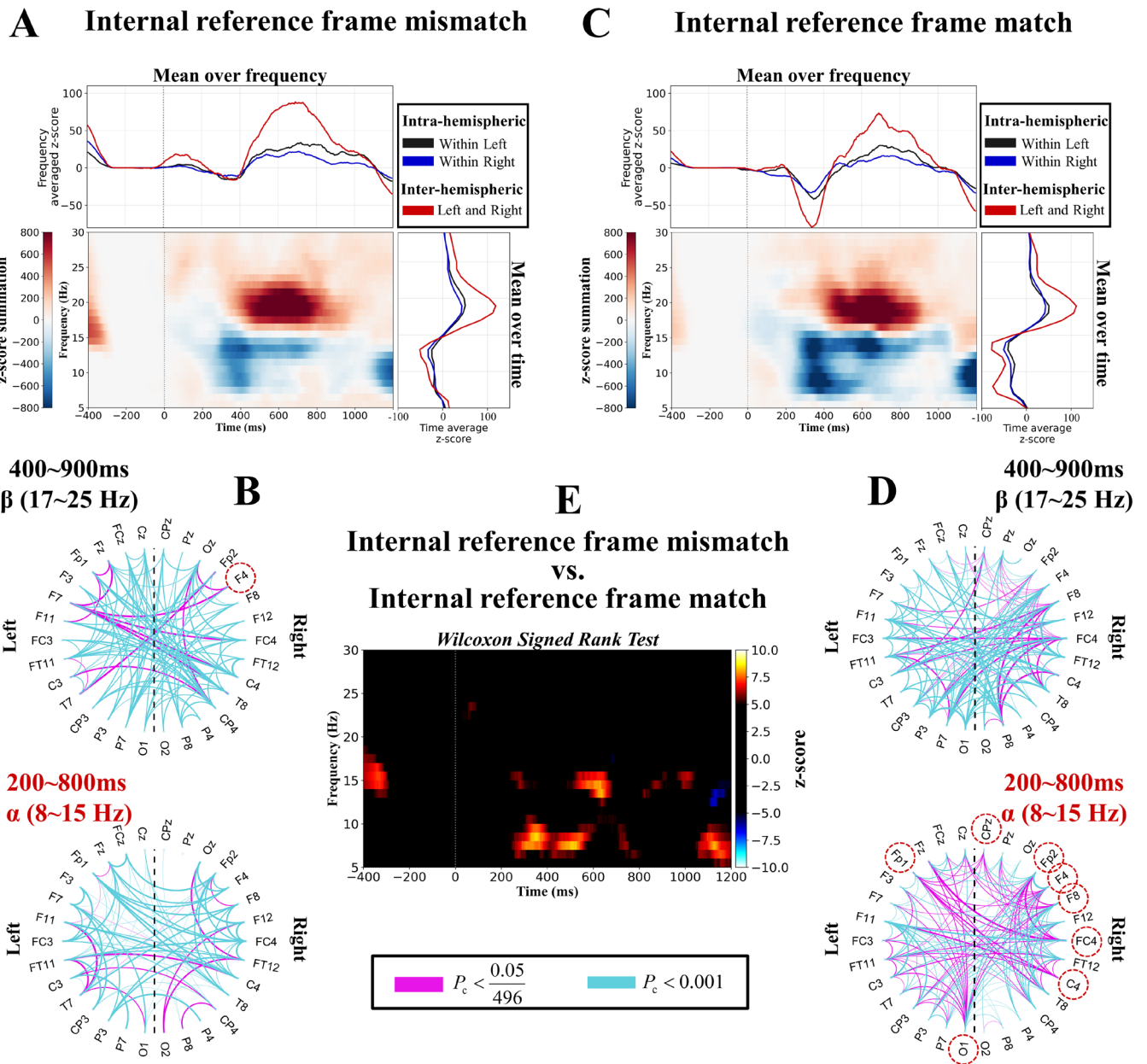
FIGURE 3 | Task-related time–frequency brain network profile under two conditions: (A) Internally reference frame mismatch and (C) Internally reference frame match. The summation of the *z*-scores of all 496 connectivity pairs that passed the nonparametric permutation test with $P_c < 0.05$ is shown. The top subplot displays the average time–frequency map across frequencies, and the right subplot shows the average across time. The value related to inter-hemispheric connections (i.e., connections between the left and right hemispheres, 169 pairs) is shown in red, and the value related to intra-hemispheric connections (i.e., connections within a hemisphere, 78 pairs) is shown in black and blue for the left and right hemispheres, respectively. The time 0 s corresponds to the delivery of the first tactile stimulus. The brain networks associated with the time windows of 200–800 ms and 400–900 ms and the frequency ranges of 8–15 Hz and 17–25 Hz are shown for (B) Internal reference frame mismatch and (D) Internal reference frame match. Magenta and cyan colors indicate the connections that pass the test with a P_c smaller than 0.05/496 (Bonferroni correction) and 0.001, respectively. In the top subplot, the curves indicate a significant increase in task-related connectivity, whereas the curves in the bottom subplot indicate a significant decrease in task-related connectivity. The red dashed circles represent network nodes where the connection density was significantly greater in one condition than in the other ($p < 0.05$) (e.g., in the beta frequency band [17–25 Hz] under the internal reference frame mismatch condition, the connection density of node F4 was greater than that under the internal reference frame match condition). (E) The *z*-scores of the Wilcoxon signed-rank test were calculated between the time–frequency connectivity maps in (A) and (C) ($P_c < 0.05$). This represents the density differences between the two conditions (mismatch vs. match) across the whole-brain network in time and frequency. Warm colors indicate mismatch > match, while cool colors indicate mismatch < match.

where *r* represents the correlation between the two variables and ΔC_α under Condition 3 represents the difference in total coupling of the alpha band between the two reference frame mismatch and match conditions, where α refers to the coupling selected from

the time window of 350–450 ms and frequency band of 8–15 Hz. ΔC_β under Condition 3 represents the difference in total coupling of the beta band between the two reference frame mismatch and match conditions, where β refers to the coupling selected from the

FIGURE 4 | Task-related time–frequency brain network profile for two conditions: (A and B) external reference frame mismatch and (C and D) external reference frame match. (E) Whole-brain network density differences between external reference frame mismatch and external reference frame match. The remaining descriptions of the figure are the same as those in Figure 3.

time window of 610–770 ms and frequency band of 17–19 Hz. ΔAcc represents the difference in accuracy between the two reference frame mismatch and match conditions.

3 | Results

We calculated the WPLI values in pairwise nondirectional coupling between the 32 EEG channels over time as well as the frequency for each participant. The WPLI was normalized at each frequency row (Figure 2B, normalized WPLI). For each time–frequency bin, we subsequently computed the t statistic against the prestimulus median at the same frequency for each participant ($p < 0.05$) (Figure 2D and Equation 3). Significant time–frequency

clusters were then extracted via a nonparametric permutation test ($P_c < 0.05/496$, 0.001, and 0.05) (Figure 2E), thereby yielding the task-related time–frequency profile of the neural oscillation.

3.1 | Condition 1: Internal Reference Frame Mismatch Versus Internal Reference Frame Match

As shown in Figure 3A,C, the neural oscillation across the whole-brain network revealed that the alpha band (8–15 Hz) significantly decreased at approximately 400 ms and that the beta band (17–25 Hz) significantly increased at approximately 600 ms, regardless of whether the internal reference frames were mismatched or matched ($P_c < 0.05$). Compared with the internal
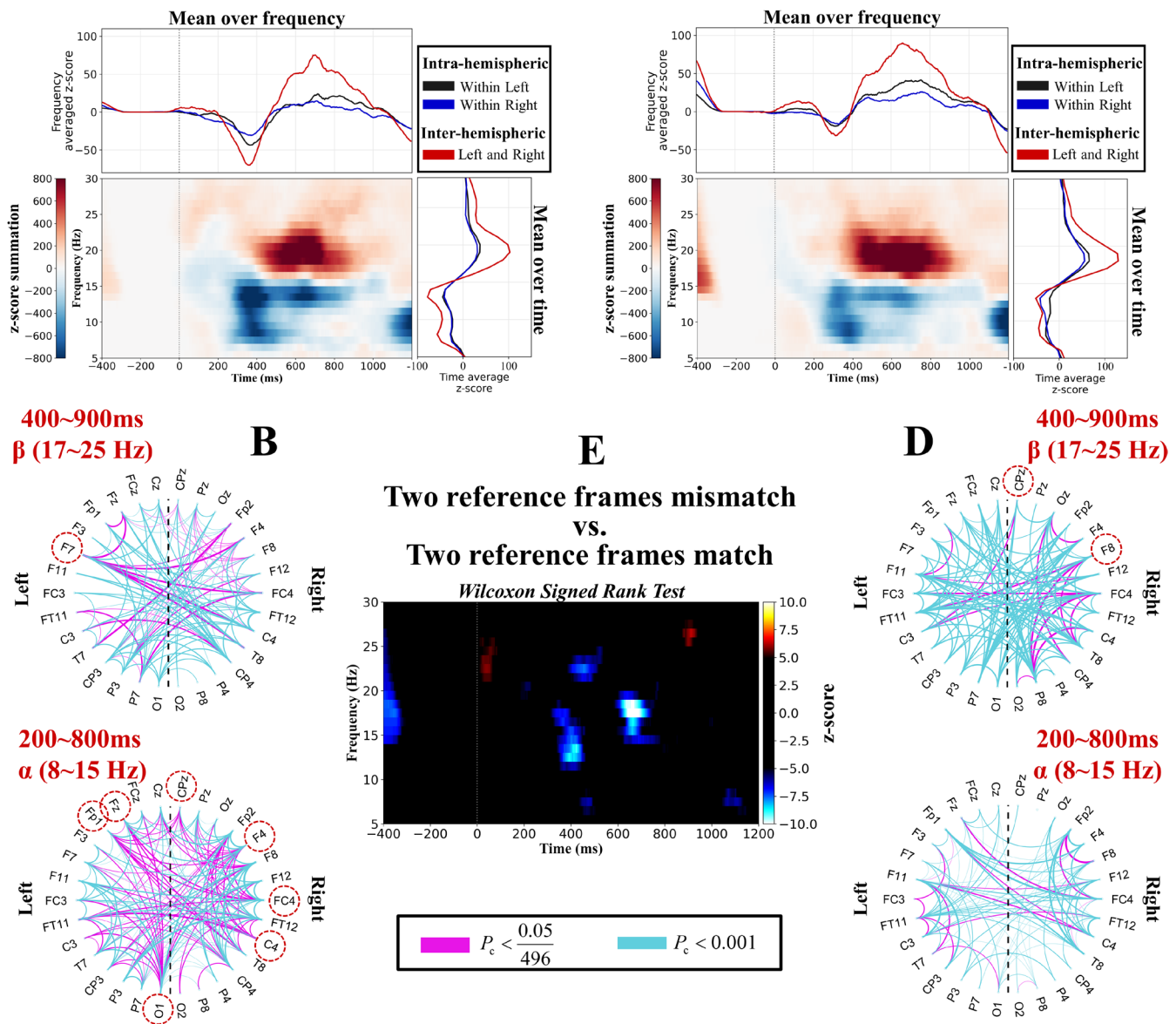
FIGURE 5 | Task-related time–frequency brain network profile for two conditions: (A and B) two reference frames mismatch and (C and D) two reference frames match. (E) Whole-brain network density differences between two reference frames mismatch and two reference frames match. The remaining descriptions of the figure are the same as those of Figure 3.

reference frame match condition, the alpha band was significantly greater under the internal reference frame mismatch condition ($P_c < 0.05$) (Figure 3E). This result indicated that the alpha band played a more important role when the internal reference frame was mismatched than when it was matched.

Next, we investigated the network connectivity density across the whole-brain network, as shown in Figure 3B,D. In the alpha band, the connectivity density was greater under the internal reference frame match condition than under the internal reference frame mismatch condition (bottom of Figure 3B,D). We also explored the task-related connectivity patterns across the whole-brain networks, and we observed that the inter-hemispheric connectivity ratios (left and right) were greater than the intra-hemispheric connectivity ratios (within left and right) in the

upper and right parts of Figure 3A,C. This result suggested that the human brain utilized inter-hemispheric connectivity to process internal reference frames.

Finally, we investigated whether the connectivity density of each electrode differed significantly between the two conditions. We found that in the alpha band, electrodes FP1, FP2, F4, F8, FC4, C4, CPz, and O1 exhibited greater connectivity density in the brain network under the internal reference frame match condition than under the mismatch condition ($p < 0.05$) (red dashed circles in Figure 3D). In the beta band, electrode F4 presented greater connectivity density than the other electrodes did under the mismatch condition compared with the match condition ($p < 0.05$) (red dashed circles in Figure 3B). The majority of these electrodes were located

in the right hemisphere. Overall, these results suggest that when the brain integrates the internal reference frame, inter-hemispheric connectivity increases, and compared with the internal reference frame match condition, the brain predominantly relies on modulating alpha band oscillations to process the internal reference frame mismatch.

3.2 | Condition 2: External Reference Frame Mismatch Versus External Reference Frame Match

As shown in Figure 4A,C, the neural oscillation across the whole-brain network revealed that the alpha band (8–15 Hz) significantly decreased at approximately 400 ms and that the beta band (17–25 Hz) significantly increased at approximately 600 ms, regardless of whether the external reference frame was a mismatch or a match ($P_c < 0.05$). In the alpha band, the initial decrease in neural oscillation was greater under the match condition (approximately 300 ms), but later (approximately 600 ms), the decrease was more pronounced under the mismatch condition ($P_c < 0.05$) (Figure 4E). In the beta band, the neural oscillation showed a stronger increase under the match condition ($P_c < 0.05$) (Figure 4E). This result indicated that the alpha band and the late beta band played a more important role when the external reference frame was mismatched than when it was matched.

Next, we investigated the network connectivity density across the whole-brain network, as shown in Figure 4B,D. In the alpha band, the connectivity density was greater under the external reference frame mismatch condition than under the external reference frame match condition (bottom of Figure 4B,D). To explore the task-related connectivity patterns across the whole-brain networks, we also observed that the inter-hemispheric connectivity ratios (left and right) were greater than the intra-hemispheric ratios (within left and right) in the upper and right parts of Figure 4A,C. This result suggested that the human brain utilizes inter-hemispheric connectivity to process external reference frames.

Finally, we investigated whether the connectivity density of each electrode differed significantly between the two conditions. We found that in the alpha band, electrodes FP1, F4, FC4, CPz, and O1 exhibited greater connectivity density in the brain network under the mismatch condition than under the match condition ($p < 0.05$) (red dashed circles in Figure 4B). In the beta band, electrodes FC4, F8, and CPz presented greater connectivity density under the match condition than under the mismatch condition ($p < 0.05$) (red dashed circles in Figure 4D). The majority of these electrodes were located in the right hemisphere. Overall, these results indicate that when the brain integrates the external reference frame, inter-hemispheric connectivity increases, and compared with the external reference frame match condition, the brain predominantly relies on modulating alpha and late beta band oscillations to process the external reference frame mismatch.

3.3 | Condition 3: Two Reference Frames Mismatch Versus Two Reference Frames Match

As shown in Figure 5A,C, the neural oscillation across the whole-brain network revealed that the alpha band (8–15 Hz) significantly decreased at approximately 400 ms and that the

beta band (17–25 Hz) significantly increased at approximately 600 ms, regardless of whether the internal or external reference frame was mismatched or matched ($P_c < 0.05$). In the alpha band, the neural oscillation decreased more under the mismatch condition (approximately 400 ms), whereas in the beta band, it increased more under the match condition (approximately 700 ms) ($P_c < 0.05$) (Figure 5E). This result indicated that the early alpha and late beta bands played a more important role when the two reference frames were mismatched than when they were matched.

Next, we investigated the connectivity density across the whole-brain network, as shown in Figure 5B,D. In the alpha band, the network connectivity density was greater under the internal and external reference frame mismatch condition than under the match condition, whereas in the beta band, the network connectivity density was lower under the internal and external reference frame mismatch condition than under the match condition. Additionally, to explore the task-related connectivity patterns across the whole-brain networks, we also observed that the inter-hemispheric connectivity ratios (left and right) were greater than the intra-hemispheric ratios (within left and right) in the upper and right parts of Figure 5A,C. This result suggested that the human brain utilized inter-hemispheric connectivity to process the internal and external reference frames.

Finally, we investigated whether the connectivity density of each electrode differed significantly between the two conditions. We found that in the alpha band, electrodes FP1, F4, Fz, FC4, C4, CPz, and O1 exhibited greater connectivity density in the brain network under the mismatch condition than under the match condition ($p < 0.05$) (red dashed circles at the bottom of Figure 5B). In the beta band, electrode F7 showed greater connectivity density under the mismatch condition, whereas electrodes F8 and CPz showed greater connectivity density under the match condition ($p < 0.05$) (red dashed circles at the top of Figure 5B,D). The majority of these electrodes were located in the right hemisphere. Overall, these results indicate that when the brain integrates the internal and external reference frame, inter-hemispheric connectivity increases, and compared with the internal and external reference frame match condition, the brain predominantly relies on modulating early alpha and late beta band oscillations to process the internal and external reference frame mismatch.

3.4 | Correlation Analysis

Finally, Pearson correlation analysis was used to explore the relationships between the significant differences in the alpha and beta bands and the differences in accuracy. For accuracy (mean ± SD), the internal reference frame mismatch was 0.87 ± 0.07, and the internal reference frame match was 0.81 ± 0.08; the external reference frame mismatch was 0.84 ± 0.07, and the external reference frame match was 0.84 ± 0.08; and the two reference frames mismatch were 0.84 ± 0.07, and the two reference frames match were 0.84 ± 0.08.

Under each condition, we explored the relationship between the significant differences in the alpha and beta bands and the differences in accuracy via Pearson correlation analysis. Figure 6A
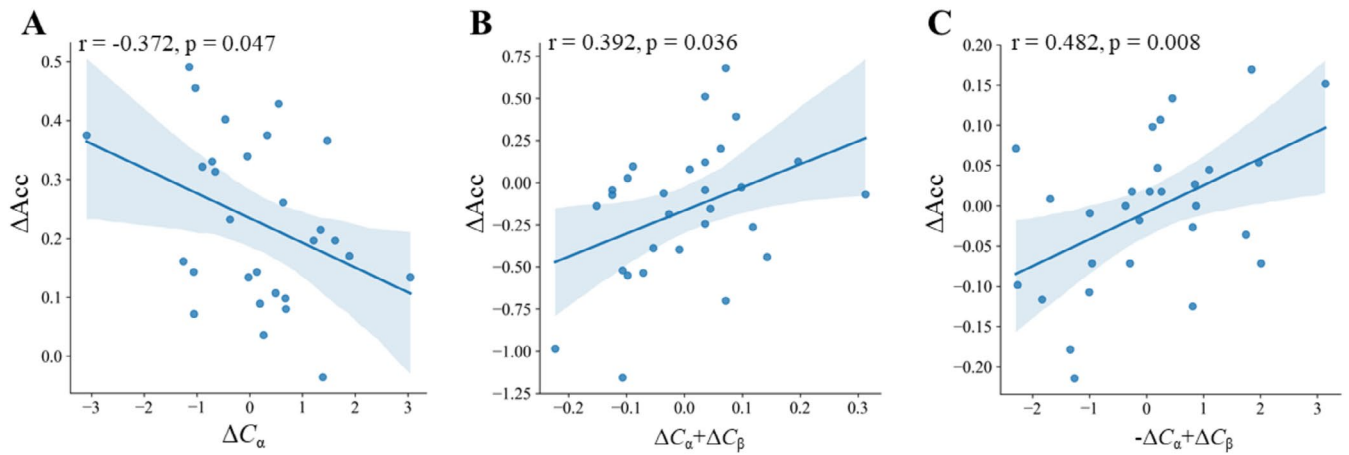
FIGURE 6 | Pearson correlation analysis between the significant differences in the alpha and beta bands and the differences in accuracy. (A) Correlation analysis between the difference in the total coupling values of the alpha band under the internal reference frame mismatch and internal reference frame match conditions and the difference in accuracy between the two conditions. α refers to the coupling values selected from the time window of 350–800 ms and the frequency band of 8–10 Hz, as well as from the time window of 520–660 ms and the frequency band of 13–15 Hz. (B) Correlation analysis between the difference in the total coupling values of the alpha and beta bands under the external reference frame mismatch and external reference frame match conditions and the difference in accuracy between the two conditions. α refers to the coupling values selected from the time window of 200–700 ms and the frequency band of 13–15 Hz, and β refers to the coupling values selected from the time window of 750–900 ms and the frequency band of 17–25 Hz. (C) Correlation analysis between the difference in the total coupling values of the alpha and beta bands under the two reference frames mismatch and two reference frames match conditions and the difference in accuracy between the two conditions. α refers to the coupling values selected from the time window of 350–450 ms and the frequency band of 8–15 Hz, and β refers to the coupling values selected from the time window of 610–770 ms and the frequency band of 17–19 Hz.

shows the correlation results under Condition 1: ΔC_α was negatively correlated with ΔAcc ($r[29] = -0.372$, $p = 0.047$), meaning that in the alpha frequency band, as the difference in total coupling values between the internal reference frame mismatch and match increased, the accuracy difference between the two conditions decreased. Figure 6B shows the correlation results under Condition 2: $\Delta C_\alpha + \Delta C_\beta$ was positively correlated with ΔAcc ($r[29] = 0.392$, $p = 0.036$), meaning that in the alpha and late beta frequency bands, as the difference in total coupling values between the external reference frame mismatch and match increased, the accuracy difference between the two conditions increased. Figure 6C shows the correlation results under Condition 3: $-\Delta C_\alpha + \Delta C_\beta$ was positively correlated with ΔAcc ($r[29] = 0.482$, $p = 0.008$), meaning that in the early alpha and late beta frequency bands, as the difference in total coupling values between internal and external reference frame mismatch and match increased, the accuracy difference between the two conditions increased.

These results suggest that during the regulation of different reference frame mismatch, the brain relies on oscillatory activity in different frequency bands. In the case of internal reference frame mismatch, the brain predominantly relies on modulation of the alpha band; in external reference frame mismatch, both alpha and late beta band oscillations are involved; and when processing the mismatch between internal and external reference frames, the synergistic modulation of early alpha and late beta band oscillations plays a crucial role.

4 | Discussion

In this study, we observed that the alpha band oscillation significantly decreased and the beta band oscillation significantly

increased under the internal reference frame mismatch and match conditions, the external reference frame mismatch and match conditions, and the internal and external reference frame mismatch and match conditions (Figures 3A,C, 4A,C, and 5A,C, respectively). Correlation analysis suggested that, during internal reference frame mismatch, the brain predominantly relied on modulation of the alpha band; during external reference frame mismatch, both alpha and late beta band activities were involved; and when processing the mismatch between internal and external reference frames, synergistic modulation of early alpha and late beta band oscillations was required (Figure 6). Differences in coupling predict behavioral performance, and the two are closely related. These results suggest that the alpha and beta bands play important roles in regulating the brain's integration of internal and external reference frames. On the one hand, the decrease in alpha band oscillation is closely related to cognitive control over irrelevant information suppression. This decrease helps humans optimize the allocation of cognitive resources, thereby enabling the brain to focus more on task-relevant information processing (Jensen and Mazaheri 2010; Klimesch 2012). On the other hand, the increase in beta band oscillation is closely related to sensorimotor integration and attention maintenance (Engel and Fries 2010; Kilavik et al. 2013). Moreover, the increase in beta band activity helps us promote communication between cortical regions (Kilavik et al. 2013). Recent studies have shown that when hands are crossed, beta band communication is crucial for making accurate judgments (Moharramipour et al. 2023). Rueda-Delgado et al. also reported that an increase in task difficulty during a bimanual coordination task is correlated with greater beta band power and stronger inter-hemispheric connectivity (Rueda-Delgado et al. 2017). This correlation might explain why we observed

increased beta band coupling under each condition and why the brain mainly utilized inter-hemispheric connectivity to process the modified TOJ task.

By comparing the significant connectivity densities across electrode sites under each pair of conditions, we found that these electrodes were predominantly located in the right hemisphere, which may be related to the spatial processing advantages of this hemisphere (Hugdahl 2013; Shulman et al. 2010) In summary, the decrease in interactions in the alpha band and the increase in interactions in the beta band complement each other, thus enabling the brain to suppress irrelevant information while enhancing the processing of task-relevant information, thereby achieving precise tactile spatial localization.

When investigating internal reference frame mismatch, we found that the brain relies more heavily on a decrease in alpha band oscillation when processing the internal reference frame. The decrease in alpha band oscillation reflects decreased inhibitory control over internal states, which enables the brain to release more neural resources for integrating and processing reference frame information (Foxe and Snyder 2011). At the beginning of the experimental design, we aimed to study brain network interactions under internal reference frame mismatch. However, an interesting phenomenon emerged in the results: compared with the internal reference frame mismatch condition, the internal reference frame match condition resulted in a more significant decrease in alpha band coupling and greater network connectivity (Figure 3B,D,E). These findings may be attributed to the fact that coordination of the different side limbs is more frequent in daily life, leading to increased processing complexity under the match (same side) condition. This increased complexity is consistent with the findings of Nakagawa et al., who reported that ipsilateral limb coordination activates the auxiliary motor areas more strongly than contralateral coordination does (Nakagawa et al. 2016).

When investigating external reference frame mismatch, we found that the alpha and beta bands played important roles in processing external reference frames. This result is similar to how the brain integrates internal and external reference frames, supporting the concept of tactile remapping: the brain maps internal reference frame information to the external reference frame, allowing for precise tactile spatial localization. We also found that a greater increase in beta band oscillation was observed under the external reference frame match conditions than under the external reference frame mismatch conditions. This difference may be due to the fact that the stimulated hand and foot are on the same side, with a smaller spatial distance, which increases the need for sustained attention to the target area, thereby promoting an increase in beta band activity (Heed and Roeder 2010).

When investigating internal and external reference frame mismatch, we found that, compared with the match condition, early alpha oscillations and late beta oscillations were reduced (Figure 5E). Schicke and Röder suggested that when internal and external reference frames conflict, task complexity increases, leading to a greater cognitive load and the depletion of attentional resources (Schicke and Röder 2006).

The reduction in early alpha oscillations further supports the idea that diminished alpha band activity plays a crucial role in enhancing task processing under conditions of high cognitive load (Jensen and Mazaheri 2010). Moreover, the increase in cognitive load may also prevent the brain from maintaining sustained cognitive states during the later stages of task performance, as reflected by the decrease in beta oscillations in the later task phases (Engel and Fries 2010; Yu et al. 2021). Specifically, when the brain can maintain cognitive stability while processing internal and external reference frame mismatch, more attentional resources are required to regulate the conflict between internal and external information. However, when the cognitive load becomes too high, the brain is unable to sustain its original neural synchronization state, leading to a reduction in beta band oscillations.

In our experimental design, the inclusion of a different numbers of males and females may have influenced the results. Future studies should include a larger equal number of males and females to verify the results. Second, the spatial resolution of the task-related EEG data we collected was limited. Future studies should employ functional magnetic resonance imaging to gain deeper insights into the brain mechanisms involved in the integration of internal and external reference frames. Finally, we stimulated relatively distal sites on the body (the second joint of the middle finger and above the ankle). Future research should investigate whether the effects observed are also evident at other body sites, such as more proximal regions of the limbs or even nonlimb areas.

5 | Conclusion

In summary, this study explored neural oscillation when the human brain integrated internal and external reference frames for accurate tactile spatial localization. The alpha and beta band oscillations with inter-hemispheric connectivity contributed to the processing of the internal and external reference frames. These findings could provide insights into the effective use of neural oscillation-based assessments for neurorehabilitation.

Conflicts of Interest

The authors declare no conflicts of interest.

Data Availability Statement

The data that support the findings of this study are available on request from the corresponding author. The data are not publicly available due to privacy or ethical restrictions.

References

Alouit, A., M. Gavaret, C. Ramdani, P. G. Lindberg, and L. Dupin. 2024. "Cortical Activations Associated With Spatial Remapping of Finger Touch Using EEG." *Cerebral Cortex* 34, no. 4: bhae161.

Azañón, E., M.-P. Stenner, F. Cardini, and P. Haggard. 2015. "Dynamic Tuning of Tactile Localization to Body Posture." *Current Biology* 25, no. 4: 512–517.

Badde, S., B. Röder, and T. Heed. 2019. "Feeling a Touch to the Hand on the Foot." *Current Biology* 29, no. 9: 1491–1497.e4.

Buchholz, V. N., O. Jensen, and W. P. Medendorp. 2011. "Multiple Reference Frames in Cortical Oscillatory Activity During Tactile Remapping for Saccades." *Journal of Neuroscience* 31, no. 46: 16864–16871.

Cheyne, D., W. Gaetz, L. Garnero, et al. 2003. "Neuromagnetic Imaging of Cortical Oscillations Accompanying Tactile Stimulation." *Cognitive Brain Research* 17, no. 3: 599–611.

Cohen, M. X. 2019. "A Better Way to Define and Describe Morlet Wavelets for Time–Frequency Analysis." *NeuroImage* 199: 81–86.

Engel, A. K., and P. Fries. 2010. "Beta-Band Oscillations—Signalling the Status Quo?" *Current Opinion in Neurobiology* 20, no. 2: 156–165.

Faul, F., E. Erdfelder, A.-G. Lang, and A. Buchner. 2007. "G*Power 3: A Flexible Statistical Power Analysis Program for the Social, Behavioral, and Biomedical Sciences." *Behavior Research Methods* 39, no. 2: 175–191.

Foxe, J. J., and A. C. Snyder. 2011. "The Role of Alpha-Band Brain Oscillations as a Sensory Suppression Mechanism During Selective Attention." *Frontiers in Psychology* 2: 154. https://doi.org/10.3389/fpsyg.2011.00154.

Gramfort, A., M. Luessi, E. Larson, et al. 2013. "MEG and EEG Data Analysis With MNE-Python." *Frontiers in Neuroscience* 7: 267. https://doi.org/10.3389/fnins.2013.00267.

Haggard, P., M. Taylor-Clarke, and S. Kennett. 2003. "Tactile Perception, Cortical Representation and the Bodily Self." *Current Biology* 13, no. 5: R170–R173.

Hassan, M., and F. Wendling. 2018. "Electroencephalography Source Connectivity: Aiming for High Resolution of Brain Networks in Time and Space." *IEEE Signal Processing Magazine* 35, no. 3: 81–96.

Heed, T., and E. Azañón. 2014. "Using Time to Investigate Space: A Review of Tactile Temporal Order Judgments as a Window Onto Spatial Processing in Touch." *Frontiers in Psychology* 5: 76.

Heed, T., V. N. Buchholz, A. K. Engel, and B. Röder. 2015. "Tactile Remapping: From Coordinate Transformation to Integration in Sensorimotor Processing." *Trends in Cognitive Sciences* 19, no. 5: 251–258.

Heed, T., and B. Roeder. 2010. "Common Anatomical and External Coding for Hands and Feet in Tactile Attention: Evidence From Event-Related Potentials." *Journal of Cognitive Neuroscience* 22: 184–202.

Hollander, M., D. A. Wolfe, and E. Chicken. 2013. *Nonparametric Statistical Methods*. John Wiley & Sons.

Hugdahl, K. 2013. "Visual–Spatial Information Processing in the Two Hemispheres of the Brain is Dependent on the Feature Characteristics of the Stimulus." *Frontiers in Neuroscience* 7: 10. https://doi.org/10.3389/fnins.2013.00010.

Imperatori, L. S., M. Betta, L. Cecchetti, et al. 2019. "EEG Functional Connectivity Metrics wPLI and wSMI Account for Distinct Types of Brain Functional Interactions." *Scientific Reports* 9, no. 1: 8894.

Jensen, O., and A. Mazaheri. 2010. "Shaping Functional Architecture by Oscillatory Alpha Activity: Gating by Inhibition." *Frontiers in Human Neuroscience* 4: 186. https://doi.org/10.3389/fnhum.2010.00186.

Kilavik, B. E., M. Zaepffel, A. Brovelli, W. A. MacKay, and A. Riehle. 2013. "The Ups and Downs of Beta Oscillations in Sensorimotor Cortex." *Experimental Neurology* 245: 15–26.

Klimesch, W. 2012. "Alpha-Band Oscillations, Attention, and Controlled Access to Stored Information." *Trends in Cognitive Sciences* 16, no. 12: 606–617.

Lau, T. M., J. T. Gwin, K. G. McDowell, and D. P. Ferris. 2012. "Weighted Phase Lag Index Stability as an Artifact Resistant Measure to Detect Cognitive EEG Activity During Locomotion." *Journal of Neuroengineering and Rehabilitation* 9, no. 1: 47.

Maris, E., and R. Oostenveld. 2007. "Nonparametric Statistical Testing of EEG- and MEG-Data." *Journal of Neuroscience Methods* 164, no. 1: 177–190.

Moharramipour, A., T. Takahashi, and S. Kitazawa. 2023. "Distinctive Modes of Cortical Communications in Tactile Temporal Order Judgment." *Cerebral Cortex* 33, no. 6: 2982–2996.

Morales, S., and M. E. Bowers. 2022. "Time–Frequency Analysis Methods and Their Application in Developmental EEG Data." *Developmental Cognitive Neuroscience* 54: 101067.

Nakagawa, K., S. Kawashima, N. Mizuguchi, and K. Kanosue. 2016. "Difference in Activity in the Supplementary Motor Area Depending on Limb Combination of Hand–Foot Coordinated Movements." *Frontiers in Human Neuroscience* 10: 499. https://doi.org/10.3389/fnhum.2016.00499.

Oldfield, R. C. 1971. "The Assessment and Analysis of Handedness: The Edinburgh Inventory." *Neuropsychologia* 9, no. 1: 97–113.

O'Neill, G. C., P. Tewarie, D. Vidaurre, L. Liuzzi, M. W. Woolrich, and M. J. Brookes. 2018. "Dynamics of Large-Scale Electrophysiological Networks: A Technical Review." *NeuroImage* 180: 559–576.

Overvliet, K. E., E. Azañón, and S. Soto-Faraco. 2011. "Somatosensory Saccades Reveal the Timing of Tactile Spatial Remapping." *Neuropsychologia* 49, no. 11: 3046–3052.

Penfield, W., and E. Boldrey. 1937. "Somatic Motor and Sensory Representation in the Cerebral Cortex of Man as Studied by Electrical Stimulation." *Brain* 60, no. 4: 389–443.

Ritterband-Rosenbaum, A., R. Hermosillo, G. Kroliczak, and P. van Donkelaar. 2014. "Hand Position-Dependent Modulation of Errors in Vibrotactile Temporal Order Judgments: The Effects of Transcranial Magnetic Stimulation to the Human Posterior Parietal Cortex." *Experimental Brain Research* 232, no. 6: 1689–1698.

Rocchi, L., E. Casula, P. Tocco, A. Berardelli, and J. Rothwell. 2016. "Somatosensory Temporal Discrimination Threshold Involves Inhibitory Mechanisms in the Primary Somatosensory Area." *Journal of Neuroscience* 36, no. 2: 325–335.

Roux, F., I. Djidjeli, and J. Durand. 2018. "Functional Architecture of the Somatosensory Homunculus Detected by Electrostimulation." *Journal of Physiology* 596, no. 5: 941–956.

Rueda-Delgado, L. M., E. Solesio-Jofre, D. Mantini, P. Dupont, A. Daffertshofer, and S. P. Swinnen. 2017. "Coordinative Task Difficulty and Behavioural Errors Are Associated With Increased Long-Range Beta Band Synchronization." *NeuroImage* 146: 883–893.

Ruxton, G. D. 2006. "The Unequal Variance *t*-Test is an Underused Alternative to Student's *t*-Test and the Mann–Whitney U test." *Behavioral Ecology* 17, no. 4: 688–690.

Sambo, C. F., D. M. Torta, A. Gallace, M. Liang, G. L. Moseley, and G. D. Iannetti. 2013. "The Temporal Order Judgement of Tactile and Nociceptive Stimuli is Impaired by Crossing the Hands Over the Body Midline." *Pain* 154, no. 2: 242–247.

Schicke, T., and B. Röder. 2006. "Spatial Remapping of Touch: Confusion of Perceived Stimulus Order Across Hand and Foot." *Proceedings of the National Academy of Sciences* 103, no. 31: 11808–11813.

Serino, A., and P. Haggard. 2010. "Touch and the Body." *Neuroscience & Biobehavioral Reviews* 34, no. 2: 224–236.

Shore, D. I., E. Spry, and C. Spence. 2002. "Confusing the Mind by Crossing the Hands." *Cognitive Brain Research* 14, no. 1: 153–163.

Shulman, G. L., D. L. W. Pope, S. V. Astafiev, M. P. McAvoy, A. Z. Snyder, and M. Corbetta. 2010. "Right Hemisphere Dominance During Spatial Selective Attention and Target Detection Occurs Outside the Dorsal Frontoparietal Network." *Journal of Neuroscience* 30, no. 10: 3640–3651.

Stam, C. J., G. Nolte, and A. Daffertshofer. 2007. "Phase Lag Index: Assessment of Functional Connectivity From Multi Channel EEG and MEG With Diminished Bias From Common Sources." *Human Brain Mapping* 28, no. 11: 1178–1193.

Tamè, L., E. Azañón, and M. R. Longo. 2019. "A Conceptual Model of Tactile Processing Across Body Features of Size, Shape, Side, and Spatial Location." *Frontiers in Psychology* 10: 291. https://doi.org/10.3389/fpsyg.2019.00291.

Vinck, M., R. Oostenveld, M. van Wingerden, F. Battaglia, and C. M. A. Pennartz. 2011. "An Improved Index of Phase-Synchronization for Electrophysiological Data in the Presence of Volume-Conduction, Noise and Sample-Size Bias." *NeuroImage* 55, no. 4: 1548–1565.

Williamson, J. N., W. A. Sikora, S. A. James, et al. 2022. "Cortical Reorganization of Early Somatosensory Processing in Hemiparetic Stroke." *Journal of Clinical Medicine* 11, no. 21: 6449.

Xie, W., R. T. Toll, and C. A. Nelson. 2022. "EEG Functional Connectivity Analysis in the Source Space." *Developmental Cognitive Neuroscience* 56: 101119.

Yamamoto, S., and S. Kitazawa. 2001. "Reversal of Subjective Temporal Order Due to Arm Crossing." *Nature Neuroscience* 4: 759–765.

Yu, S., M. Mückschel, and C. Beste. 2021. "Event-Related Synchronization/Desynchronization and Functional Neuroanatomical Regions Associated With Fatigue Effects on Cognitive Flexibility." *Journal of Neurophysiology* 126, no. 2: 383–397.